# ASIS—A New Air–Sea Interaction Spar Buoy: Design and Performance at Sea

HANS C. GRABER

*Rosenstiel School of Marine and Atmospheric Science, University of Miami, Miami, Florida*

EUGENE A. TERRAY

*Woods Hole Oceanographic Institution, Woods Hole, Massachusetts*

MARK A. DONELAN, WILLIAM M. DRENNAN, AND JOHN C. VAN LEER

*Rosenstiel School of Marine and Atmospheric Science, University of Miami, Miami, Florida*

DONALD B. PETERS

*Woods Hole Oceanographic Institution, Woods Hole, Massachusetts*

ABSTRACT

This paper describes a new, compact buoy, the Air–Sea Interaction Spar (ASIS), capable of reliably and accurately measuring directional wave spectra, atmospheric surface fluxes, and radiation in the the open ocean. The ASIS buoy is a stable platform and has low flow disturbance characteristics in both atmospheric and oceanic surface boundary layers. The buoy has been deployed for sea trials in the waters off Miami, Florida; in the northeastern region of the Gulf of Mexico; and in the northwestern Mediterranean. The acquired measurements of directional wave spectra, momentum and heat fluxes, and profile data—as well as general meteorological and oceanographic parameters—obtained from the buoy are well suited for enhancing research on air–water interfacial processes, wave dynamics, remote sensing, and gas transfer. In this paper the design is described and the performance of the buoy using field data is characterized.

## 1. Introduction

There is a growing need for high-resolution wave directional measurements at sea, arising in diverse fields such as wave dynamics, air–sea coupling, gas exchange, and microwave and acoustic remote sensing. Wave properties affect the coupling of atmosphere and ocean in many ways and coincident and simultaneous measurements of the fluxes of mass, momentum, and energy are required to fully understand the coupling mechanisms, to interpret remote sensing measurements and to link global climate models of ocean and atmosphere.

Most observations of directional wave properties at sea are derived from moored surface-following buoys, such as heave–pitch–roll buoys or triaccelerometer buoys. These devices measure the first three (complex) coefficients of the Fourier transform of the directional distribution, and hence provide coarse directional resolution (e.g., they cannot resolve multimodal seas in a model-independent way). Furthermore, such buoys are inherently incapable of resolving waves smaller than their characteristic dimensions, typically $O(1–10$ m). However, many aspects of air–sea interaction and remote sensing are governed by meter to centimeter long waves. In particular, various active microwave remote sensing techniques, such as HF and synthetic aperture radar, and scatterometry, depend on the backscatter from relatively short waves (determined by the Bragg resonance condition). Accurate directional wave measurements, particularly in the frequency range of 2–5 Hz are required for the precise interpretation of radar backscatter within the context of an improved understanding of Bragg-wave modulation (Valenzuela 1978).

The validation of remote sensing techniques also requires a detailed understanding of meteorological conditions (wind forcing, boundary layer stability, etc.). For example, scatterometry model functions are based largely on an empirical relationship between the wind speed at some reference height and the radar cross section $\sigma_o$, which, as discussed above, depends on the small-scale

*Corresponding author address:* Hans C. Graber, Division of Applied Marine Physics, Rosenstiel School of Marine and Atmospheric Science, University of Miami, 4600 Rickenbacker Causeway, Miami, FL 33149-1098.
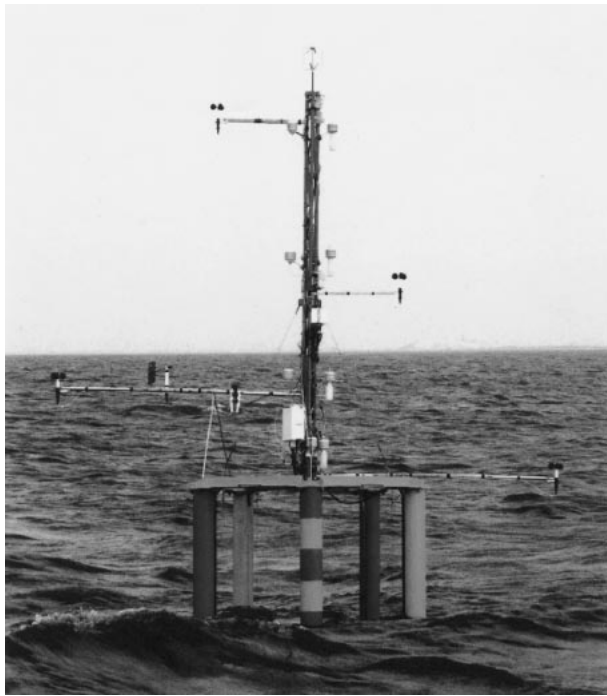E-mail: hgraber@rsmas.miami.edu

FIG. 1. Fully instrumented air–sea interaction spar (ASIS) buoy deployed at sea.
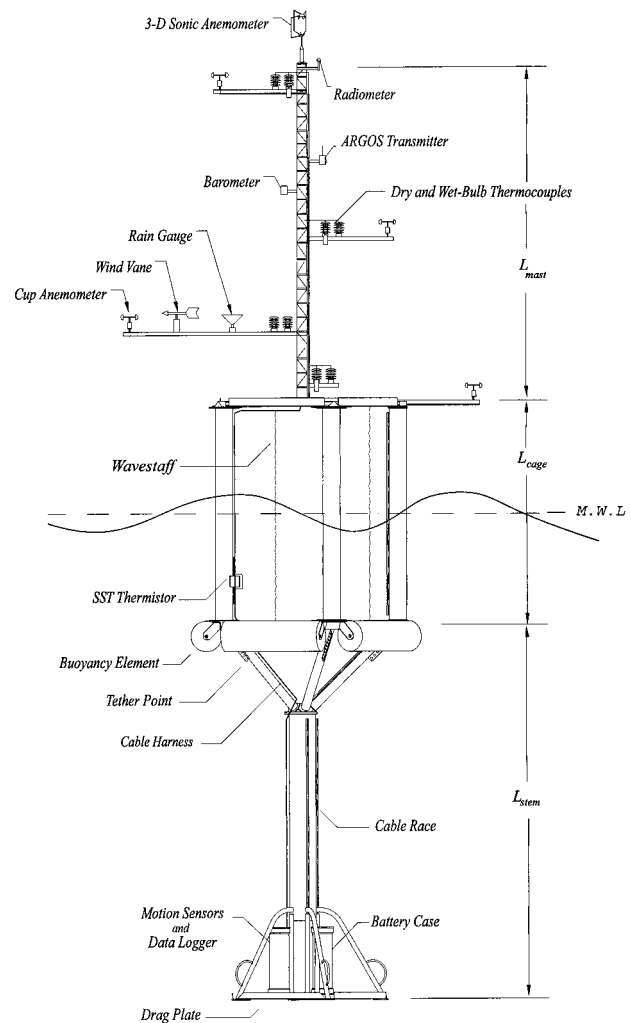


FIG. 2. Engineering drawing of the ASIS buoy showing the placement of sensors. Although the three principal lengths of the buoy can be adjusted optimally for expected sea states and current conditions, we have chosen the following lengths: $L_{mast}$ = 4.0 m, $L_{cage}$ = 2.5 m, and $L_{stem}$ = 4.5 m.

properties of the sea surface. Measurements of winds from buoys typically are adjusted in height and corrected for atmospheric stability using Monin–Obukhov (1954) similarity theory with empirical constants, that are based on measurements over land (Businger et al. 1971). However, the validity of the those flux–profile relationships has not been established over the ocean, and indeed there are reasons to believe that some modification may be necessary to account for the additional length scale imposed by the underlying waves, and the possibility of additional heat and moisture transfer processes associated with wave breaking, such as production of spray and the injection of bubbles into the water.

A buoy system capable of high-resolution measurements of waves and atmospheric fluxes, and of a size and weight to be easily portable and deployable from research vessels of intermediate size, would provide a significant improvement in current observational capability. Such a buoy, the Air–Sea Interaction Spar (ASIS), has been designed and built, and is the subject of this paper (Figs. 1 and 2). The paper is organized as follows. In section 2 we describe the criteria that guided the development of the ASIS and discuss the overall design. The selection of instrumentation and sensors is described in section 3, and the performance of the buoy at sea is summarized in section 4. Some examples of its capability of measuring waves and atmospheric fluxes, as well as a comparison with a nearby National Data Buoy Center (NDBC) 3-m discus, are presented in sec-

tion 5. A summary and discussion of the overall performance and future work are given in section 6.

## 2. The spar buoy system

Spar buoy–type platforms have been used both for research and by industry to provide stable platforms for measurements or operational activities. Large spar buoys such as the Floating Instrument Platform (FLIP) (Fisher and Spiess 1963) and the Brookhaven Spar (Mollo-Christensen and Dorman 1971) are used to measure atmospheric and oceanographic variables. The Brent Spar (Bax and de Werk 1974) and the Oryx Spar (Halkyard and Horton 1996) are utilized in the offshore oil industry as platforms for storage, off-loading, and production. A slender spar has a resonant response to wave excitation. The response at wave frequencies be-

low the resonance tends to unity, falling off rapidly as the frequency becomes large (Newman 1963; Cavaleri and Mollo-Christensen 1981). At the resonant frequency the magnitude of the response is governed by the amount of damping. In order to attain natural periods of greater than 25 s, the spars mentioned above all have lengths in excess of 30 m.

### a. The air–sea interaction spar

As discussed in the introduction, our main motivation in the development of the ASIS buoy has been to provide a platform for interfacial and near-interfacial measurements. Historically this has been a difficult problem due to the large dynamic range of surface waves. The energy containing part of the spectrum is strongly peaked at low frequencies, and it is not unusual to find the shorter waves of interest advected vertically over many meters by the low frequency wind waves and swell. From this perspective, the extreme stability of large spar buoys, such as FLIP or the Brookhaven Spar, is not entirely desirable. Surface-following buoys, such as the discus, are in this sense more desirable but have the drawback that they disturb the surface over a large area. Our approach to this problem has been one of "successive approximation," in which we seek a buoy design having a mechanical response that reduces the motion of sensors relative to the surface, while retaining the low flow disturbance characteristics of a slender spar.

Our criteria in developing the ASIS buoy are that it

1) be capable of measuring high resolution directional wave spectra;
2) provides a suitable platform for high accuracy mean and flux measurements in the air and water;
3) permits a variety of wave sensor array geometries without major modification;
4) be sufficiently stable in pitch and roll to facilitate active acoustic and microwave remote sensing and radiation flux measurements;
5) be usable in deep or coastal waters, either moored or freely drifting;
6) be durable, and easy to handle and maintain; and
7) have a cost comparable to off-the-shelf wave buoys.

The resonant frequency in heave of a spar (Newman 1977) is given by

$$\omega_o = (\rho g A(0)/M)^{1/2}, \tag{1}$$

where $A(0)$ is the waterplane area, $M$ the sum of the inertial and entrained mass, $\rho$ the water density, and $g$ the gravitational acceleration. In order that the buoy approximately follow the long waves in heave, we want to make the resonant frequency as high as possible, that is, to maximize the area of the buoy at the surface while minimizing its mass. Reducing wave interference, on the other hand, argues for a small cross section. To balance these conflicting requirements, we have constructed the upper part of the ASIS buoy from five slen-

der (20-cm diameter) vertical cylinders arranged at the vertices of a pentagon having a radius of roughly 1 m (Figs. 1 and 2). This approach distributes the buoyancy around the perimeter rather than in a central column, thus permitting each member to have a smaller diameter. For a given waterplane area, this configuration results in more wetted area (by a factor of $\sqrt{5}$), and hence somewhat more drag. The vertical columns extend roughly 1.5 m above and below the interface and are tied together several meters below the mean water line to a free-flooding vertical pipe (see Fig. 2). This central column is terminated at 6-m depth by a large pentagon-shaped drag plate made of expanded metal grating. The resulting system is overdamped in heave, pitch, and roll. We note that by separating the columns, we have also increased the restoring force in tilt over that of a simple spar, resulting in better vertical stability in the mean.

Sensors mounted on the ASIS measure quantities with respect to a moving frame of reference and must be transformed into fixed coordinates. The required measurements of the buoy motion are provided by a six degree-of-freedom inertial package consisting of "strapped-down" orthogonal triplets of accelerometers, angular rate gyros, and compass. By measuring both the motion of the buoy and the position of the surface relative to it, we eliminate the need to control or have a priori knowledge of the response function of the platform.

Surface elevation is measured using a compact array of wave height gauges within the pentagonal "cage" of the ASIS. Directional spectra of waves are estimated using the maximum likelihood method (Capon 1969). At high frequencies, directional resolution is limited by the discrete spacing of the array elements. For longer period waves the directional resolution for a given interval of time is limited by the duration of the observations, the noise level (this includes electronic noise, quantization error, and other technique-specific sources of error, such as meniscus effects in the case of surface-piercing wires), and uncertainties in the motion of the platform.

### b. The "tether" buoy

Although when freely drifting the ASIS buoy is an almost ideal surface platform, it is important in many applications to obtain a long time series at a fixed location. For this reason, the task of mooring the spar is fundamental to this project. Since the restoring force of the ASIS is relatively small (190 kgm m$^{-1}$), it is important to avoid additional downward forces that can be generated by connecting the spar to a subsurface buoy or anchor (Tasai et al. 1980). To avoid these forces—whose magnitude can vary widely depending on environmental forcing by winds, waves, and currents—we attach the spar to a surface mooring (the "tether buoy") by means of a buoyant tether. The tether consists of coil chain and wire rope with light reflecting colored plastic

TABLE 1. Instrumentation deployed during Gulf of Mexico NSCAT validation experiment. Note that altitudes are referenced to the mean sea level.

| Sensor | Manufacturer | Model | Units | Altitude (m) |
|---|---|---|---|---|
| Linear accelerometer | Columbia Research Lab. | SA-307HPTX | 3 | −6 |
| Gyrochips | Systron Donner Inertial Div. | GC1-00050-100 | 3 | −6 |
| Compass | Precision Navigation Inc. | TCM-2 | 1 | −6 |
| Wave staffs | CCIW | | 8 | ±1.25 |
| Sonic anemometer | Gill Solent | 1012R2A | 1 | 5.7 |
| Cup anemometer | R.M. Young | Gill 12005 | 4 | 1.5, 2.3, 3.4, 5.1 |
| Wet and dry thermistors | Campbell Scientific | 107 | 4 | 1.6, 2.3, 3.6, 4.9 |
| Wet and dry thermocouples | University of Washington | | 1 | 4.9 |
| Wind vane | R.M. Young | Gill 12002 | 1 | 2.4 |
| Water temperature | Campbell Scientific | 107B | 1 | −0.8 |
| Barometric pressure | Vaisala Oy | PTB101B | 1 | 2.0 |
| Pyranometer | LI-COR Inc. | LI-200SA | 1 | 5.0 |
| Rain gauge | CCIW | | 1 | 2.3 |

floats to keep the tether at the surface and improve its visibility from afar. A swivel in the middle of the 60-m-long tether is used to attach or detach the spar during deployment and recovery.

Various options for the tether buoy were explored. Traditionally, buoys have been fabricated using shipbuilding techniques with exoskeletons such as steel or fiberglass shells, which give the hull form and strength as well as resistance to damage (Steele et al. 1992; Barstow et al. 1991). We constructed the tether buoy with an aluminum core surrounded by closed cell Surlyn Ionomer foam disks. This yields a strong self-fendering buoy that is resistant to damage from collisions. Pigment, antioxidant, anti-UV and antifouling compounds were incorporated in the finished buoy. The use of a surface mooring has other advantages in that the tether buoy can carry subsurface instrumentation, such as current meters, acoustic Doppler current profilers (ADCPs), ambient noise sensors (e.g., WOTAN), and thermistor strings, spanning the entire water column. It is also a good platform for solar panels, batteries, and RF–telemetry antennas that can be used (in conjunction with an umbilical and/or an RF link to the spar) for tasks requiring high power, or long-range telemetry. To avoid mechanical fouling, the tether buoy is connected to its vertical mooring line via a swivel and is attached to the lateral tether through a torque-amplifying lever arm on top that extends beyond the diameter of the buoy. This arrangement also facilitates launching and recovery operations, and we have used it on several deployments without mishap. It apparently performs well in terms of avoiding entanglement of the tether line, even in weak currents. Graber et al. (1995) present additional discussion of the functional attributes guiding the design of the tether buoy.

The design of the mooring of the tether buoy depends on water depth. In shallow water a heavy stud-link anchor chain provides stability to the buoy through a four-part chain bridle and reduces shock loading from wave-induced motion. In deep water the restoring force is provided by an elastic mooring line below a kilometer.

## 3. Instrumentation

A summary of the sensors deployed on the ASIS during the sea trials in the Gulf of Mexico can be found in Table 1.

### a. Motion sensors

Because the wave and turbulence measurements are obtained with respect to the moving buoy, various transformations must be applied in postprocessing to transform them into "earth-referenced" coordinates (Anctil et al. 1994; Katsaros et al. 1993). The three translational and three rotational degrees of freedom of the motion of the ASIS buoy are measured using a "strapped down" inertial package, which is housed with the data acquisition system in a watertight can at the base of the buoy at roughly 6-m depth. The linear acceleration vector, $\mathbf{a}_b = (a_{b1}, a_{b2}, a_{b3})$, is sensed by three orthogonal force balance servo accelerometers (Columbia Research Laboratories, Inc.). The coordinate system adopted is a right-handed one, with $a_{b1}$, $a_{b2}$, and $a_{b3}$ positive toward the "bow," port, and upward, respectively. The vertical accelerometer is "g biased"; that is, it reads zero when at rest in a gravitational field with acceleration $g = -9.806$ m s$^{-2}$. The full-scale range is $\pm\frac{2}{3}g$ corresponding to $\pm 5$ V.

Rotational motion is sensed by three solid state Systron Donner Gyrochip angular rate gyros. These sensors use a quartz crystal oscillator whose frequency is proportional to angular velocity about an axis. One of these is paired with each of the linear accelerometers. They have a nominal range of $\pm 50°$ s$^{-1}$, corresponding to $\pm 2.5$ V. Since the performance of the rate gyros declines at lower frequencies, low frequency angular motions of pitch ($\theta$) and roll ($\phi$) are obtained from the tilt information derived from the linear accelerometers [$\theta_{lf} = -\arcsin(a_{b1}/g)$; $\phi_{lf} = \arcsin(a_{b2}/g)$]. In the case of yaw ($\psi$), low-frequency information is obtained from the heading reference provided by a compass, referenced to the level plane defined by the pitch and roll measure-

ment. The full angular motion is obtained by integrating the measured angular rates from the rate gyros and combining them, via a complementary filter, with the low-frequency information from the linear accelerometers or compass. In all cases, the crossover frequency of the complementary filter was fixed at 0.04 Hz (Brown and Hwang 1997).

### b. Wind sensors

Wind stress is estimated by direct eddy correlation from sonic anemometer measurements of winds, corrected for platform motion using the output from the inertial sensors described earlier. The sonic anemometer (Gill Systems Solent) utilizes an asymmetrical design in which the three vertical support rods making up the head are 60° apart, resulting in an unobstructed azimuthal measurement aperture of 240°. Since, when tethered, the ASIS points in the direction of the resultant of the forces due to the wind and near-surface current, the use of the asymmetrical head increases the likelihood of unimpeded flow through the sensor. The instruments are individually calibrated in a wind tunnel and are delivered with a calibration table that can be used to correct for azimuthal distortion due to wakes from the support rods and transducers (measured in steady flow). For the asymmetrical head, these corrections are small for wind directions within ±100° of the centerline. In addition to the sonic anemometer, we also measure profiles of the wind speed using cup anemometers (R. M. Young) installed at logarithmically spaced heights of 1.5, 2.3,

3.4, and 5.1 m above the mean water level. Wind direction is measured locally within the cup array at the 2.4-m level using a vane.

### c. Wave sensors

The wave sensors are capacitance wires of a design developed at the National Water Research Institute, Canada Centre for Inland Waters (CCIW). Although the ASIS provides considerable flexibility in the geometry of wave gauge arrays that can be installed, to date we have used arrays of eight wires, each roughly 2.5 m long. Five wires were installed on the faces of the pentagonal cage (at a radius of 0.93 m), midway between adjacent columns. Three additional wires, making up a right isosceles triangle with equal sides of 0.044 m, were placed with the right angle vertex on the centerline of the spar. The centerline wire together with the five on the faces of the cage make up a centered pentagonal array, which has a relatively uniform directional sensitivity for waves of length 1.8 m and greater. The small triangular array at the center is used to estimate the directional distribution of shorter waves with wavelengths from 0.1 to 1.8 m. In addition, the triangular array gives two orthogonal components of slope for waves in this range.

The actual surface elevation, $z_e$, is found by rotating the measured quantities, $z_b$, into an earth-referenced coordinate system, and then summing together the different components of motion:

$$z_e = z_b \cos\theta \cos\phi + \iint (\mathbf{a}_b \cdot [-\sin\theta, \cos\theta \sin\phi, \cos\theta \cos\phi] - g) \, dt \, dt$$

$$+ \int [L_{e2}(-\theta_t \sin\psi + \phi_t \cos\theta \cos\psi) - L_{e1}(\theta_t \cos\psi + \phi_t \cos\theta \sin\psi)] dt. \tag{2}$$

Here vector $\mathbf{L}_e = [L_{e1}, L_{e2}, L_{e3}]$ is the distance from the motion package to the water surface for a given wave staff, and subscript $t$ represents time derivative. The three terms in the equation account for correction of the wave staff measurements to true vertical, the vertical displacement of the buoy, $z_b$, itself, and the displacement due to relative rotational motion of the motion sensors, since they are not located at the surface. Further details are given in Drennan et al. (1994) and Anctil et al. (1994).

### d. Other meteorological sensors

Wet- and dry-bulb temperature measurements were made with Campbell Scientific probes, situated inside

radiation shields, at approximately 1.6, 2.3, 3.6, and 4.9 m. In addition, fast-response wet and dry thermocouples were situated just below the level of the sonic anemometer. The former sensors yield mean profiles of temperature and humidity, while the latter permit eddy correlation estimates of the fluxes of heat and moisture. A temperature probe ~1 m below the water surface recorded sea surface temperature (SST). Other sensors installed during the tests were a barometric pressure sensor (Vaisala Oy), a self-siphoning rain gauge and radiometers.

### 4. Performance at sea

After initial testing off Miami (Graber et al. 1995), the first full-scale experiment using the ASIS buoy was
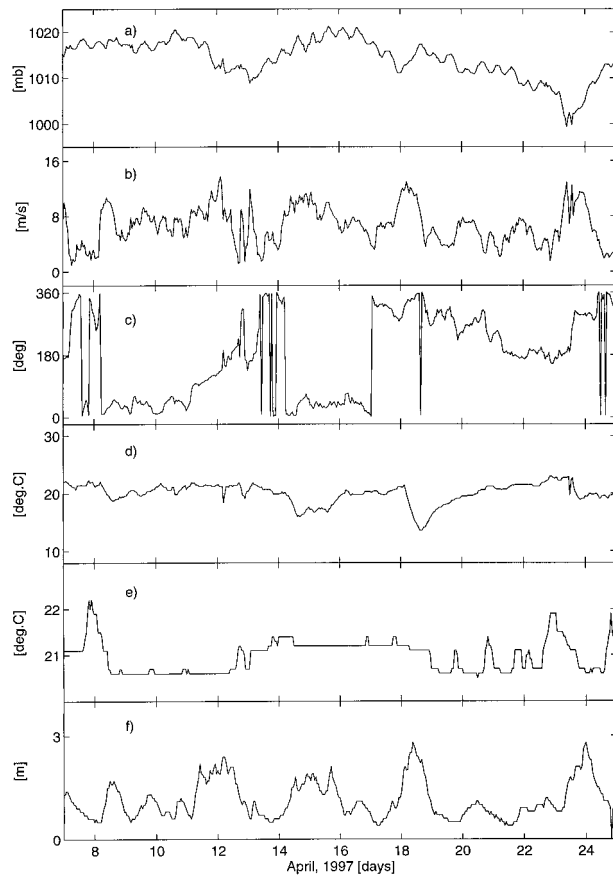
FIG. 3. Meteorological and wave conditions as reported by the nearby NDBC 3-m discus during the deployment of the ASIS buoy in the Gulf of Mexico: (a) atmospheric pressure, (b) wind speed, (c) wind direction, (d) air temperature, (e) sea surface temperature, and (f) significant wave height.
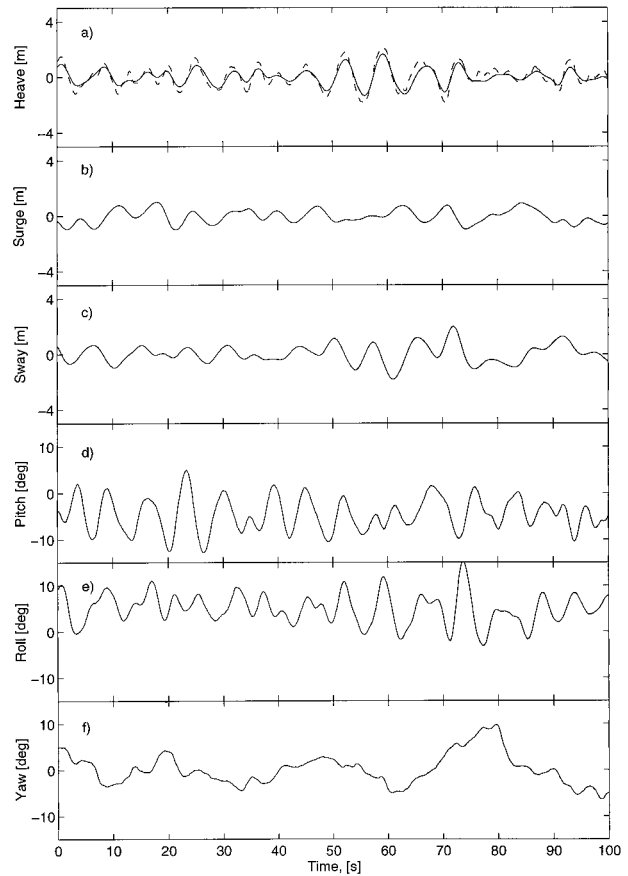
FIG. 4. Time series of 100 s of the six translational and rotational displacements of the buoy in waves of significant height of 2.92 m and wind speed of 12.7 m s$^{-1}$. The dashed line in (a) is the actual surface displacement, $z_e$ [Eq. (2)].

conducted in the Gulf of Mexico, 100 mi west of Tampa Bay, Florida. The buoy was moored to its tether buoy at 28°30'N, 84°30'W in 53 m of water from 1200 UTC 4 April to 1400 UTC 5 June 1997. Ambient conditions (7–25 April), as reported by a nearby NDBC 3-m discus buoy (station 42036), are shown in (Fig. 3).

The six degrees of freedom of the buoy's motion, the surface displacement (at eight points), and the three components of wind velocity were continuously recorded at 15 Hz. These measurements are used to recover both the buoy's response and the forcing due to waves and wind. In this section, we use these to estimate the transfer functions relating the ASIS response to the forcing.

Time series of a 100-s segment of the three linear accelerations (heave, surge, and sway) and angular motions (pitch, roll, and yaw) during the highest wave conditions encountered during this deployment (2300 UTC 23 April) are displayed in Fig. 4. Figure 4a shows the actual surface elevation, $z_e$ (dashed line), together with the heave displacement of the ASIS buoy, $z_h$ (solid). The buoy is seen to follow the long waves reasonably

well in both amplitude and phase. Surge and sway motions of the spar are shown in Figs. 4b,c. Note that surge is defined to be in the direction of the tether, which in this case is roughly 37° to the wind (which is blowing from ~315°N). As expected, the figure shows a roughly equal response in surge and sway. Angular motions (i.e., pitch, roll, and yaw) are shown in Figs. 4d–f. The standard deviations of these angles are, respectively, 3.6°, 2.8°, and 3.8° in strong winds and large waves ($H_s = 2.92$ m, $U_5 = 12.7$ m s$^{-1}$), which attests to the rotational stability of the ASIS. Note that the yawing motion of the spar is principally at lower frequencies than the waves.

Figure 5 shows an example of the surface displacement spectrum $S_{z_e z_e}$ (dashed line) and the amplitude response transfer function (solid line) of the ASIS buoy displacement in heave, $z_h$, with the incoming waves $z_e$ taken to be the principal forcing. Here, the complex transfer function is defined as

$$T = S_{z_e z_h}/S_{z_e z_e}, \qquad (3)$$

where $S$ represents the frequency spectrum or cospectrum. The response closely follows the forcing between
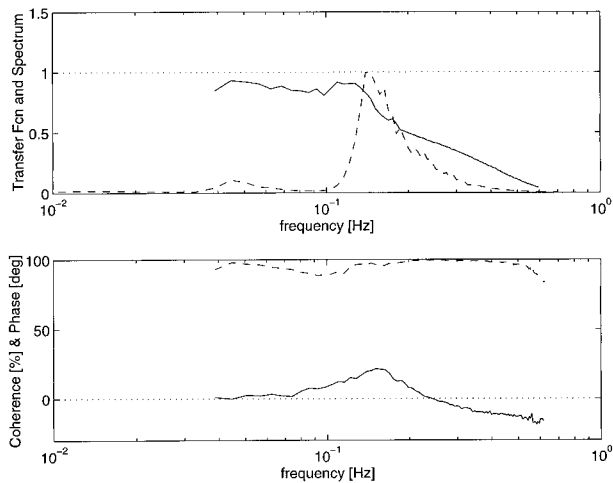
FIG. 5. Measured heave response function in waves of significant height in the range of 0.5 to 3 m. Top panel: average wave surface elevation spectrum (dashed line) and amplitude response transfer function (solid line). Bottom panel: Coherence (dashed line) and phase (solid line) between forcing and response. The phase is positive where forcing leads response and is plotted only where the coherence exceeds 80%.



FIG. 6. Expected wave staff excursion (surface elevation − buoy heave displacement) exceeded by 1% of waves as a function of sea state. Full development, $U/C_p = 0.83$ (*); $U/C_p = 1.5$ (○); $U/C_p = 2$ (+). The lower and upper dashed lines correspond to the wave staff heights used in Gulf of Mexico (model 1) and Mediterranean Sea (model 2), respectively.

0.04 and 0.12 Hz (25- to 8-s period), after which it drops off quickly to 0.2 Hz and more slowly thereafter. This can be seen more clearly in the bottom panel of Fig. 5, where we have plotted the coherence and phase angle between the waves (forcing) and heave displacement (response). The coherence is high between 0.04 and 0.6 Hz. In this region the phase rises to almost 20° at 0.15 Hz and drops off with increasing frequency, becoming negative in the higher frequencies. Negative phase angle here means that buoy response leads the forcing. This apparently paradoxical result is believed to be due to the increased dominance of the drag of the vertical orbital velocity acting principally on the horizontal cylindrical buoyancy elements at middepth—vertical velocity leads surface elevation.

This experiment exposed the ASIS buoy to waves of up to 3-m significant height for nearly two months. While this is a respectable performance during its "maiden voyage," the buoy will encounter much higher seas in future deployments. In order to make useful measurements in such sea states, the buoy must follow the long waves well enough so that the surface is always in the measurement zone of the wave staffs—any excursions beyond this region will result in "clipped" apparent waves. Using the observed transfer function (Fig. 5) we computed the expected motion of the buoy in various sea states generated using the Donelan et al. (1985) spectrum and the assumption of random phases of the components. Figure 6 shows the expected wave staff excursion (surface elevation − buoy heave displacement) exceeded by 1% of the waves versus significant height for various stages of development (inverse wave age). The lower horizontal dashed line corresponds to the length of the ASIS cage, and consequent
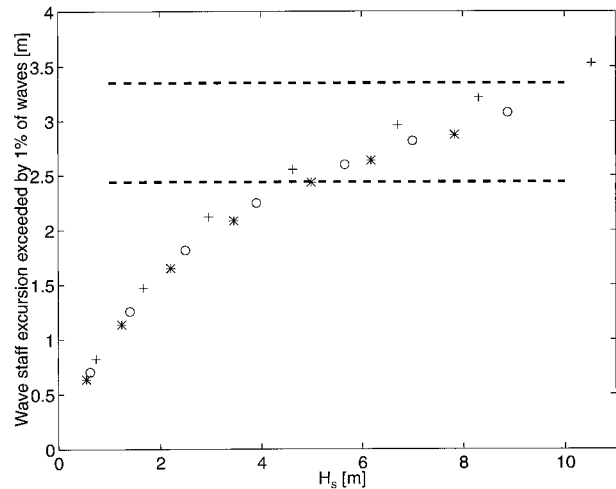
surface excursion limit, during the Gulf of Mexico deployment. It is evident that this prototype design (model 1) would suffer signal degradation due to wave staff clipping for sea states with $H_s$ over 4 m. Consequently, the buoy design was modified by extending the length by 1 m in both the cage area and the lower pipe. Again using the heave transfer function, we estimate that the new (stretched) version will not suffer significant overtopping until the significant height exceeds 10 m (Fig. 6).

This new version (model 2) was deployed in the western Mediterranean during March–April 1998 as part of the FETCH (Flux, Etat de Mer et Teledetection en Condition de Fetch Variable) experiment. During the four-week deployment, the buoy was exposed to a variety of conditions, including two mistrals, with winds up to 19 m s$^{-1}$ and waves up to 3 m $H_s$. The heave transfer function for the extended model, calculated from the FETCH data, is shown in Fig. 7. The function is similar to that of model 1, but the resonance period has been shifted from roughly 8 to 10 s. It is significant that even at the resonant frequency, the drag plate ensures that the transfer function barely exceeds 1, and remains well below 1 at higher frequencies. We expect the transfer function to approach unity at lower frequencies.

Pitch and roll transfer functions are explored in a similar way with the forcing taken as the measured slope (from the array of wave staffs) in the $x$ and $y$ directions (Fig. 8), respectively. The model 2 roll transfer function has a broad maximum of about 50% around 0.09 Hz; the pitch transfer function reaches higher values, but remains well below 1. The low amplitude of the transfer
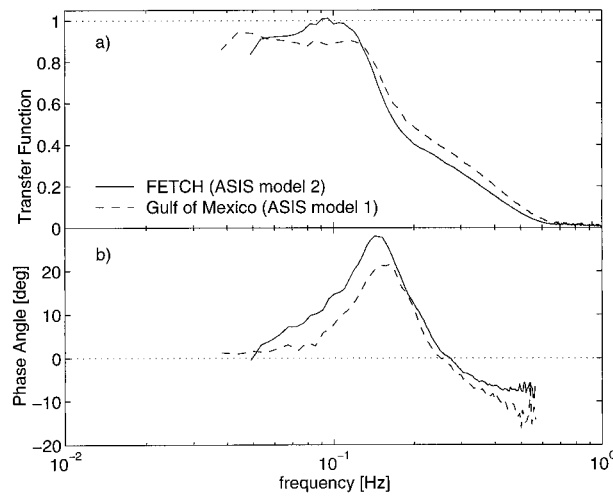
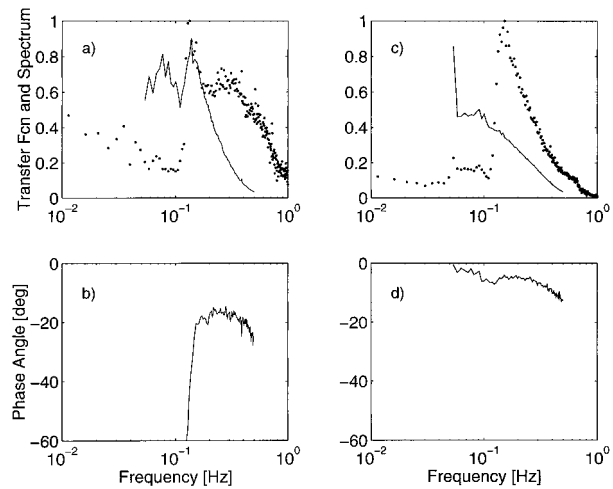FIG. 7. Measured heave response function for the two ASIS models.



FIG. 8. Measured pitch (left side) and roll (right side) transfer functions for ASIS model 2 in waves of significant height in the range of 0.5 to 3 m. Top panels: average wave surface slope spectrum (dotted line) and amplitude response transfer function (solid line). Bottom panels: Phase angle between forcing and response. The phase is positive where forcing leads response and is plotted only where the coherence exceeds 80%.

functions reflect the vertical stability of the buoy, that is, its resistance to pitching and rolling.

In order to examine the possibility of abrupt application of forces from the tether (i.e., "jerking") we consider the histograms (Fig. 9) of acceleration in the three orthogonal axes. Sudden jerks from the tether would be expected to result in large positive surge accelerations with much smaller effects in sway and heave. The histograms of Fig. 9 (for the conditions of $H_s = 2.92$) show closely Gaussian distributions of acceleration on all three axes, with surge and sway very similar in shape and with much the same standard deviation (as mentioned earlier, this is not unexpected given the buoy orientation). Heave, which is affected by buoyancy forces in addition to having a different drag profile, has a larger standard deviation, but remains Gaussian. We conclude from this that jerking of the buoy by the tether is small.

The stability of the ASIS buoy to tilting motions (i.e., in pitch and roll) is illustrated in Fig. 10a by comparing its observed rms tilt with that of the surface on scales larger than 2 m for various significant heights. The figure shows that the rms buoy tilts are smaller by a factor of about 2.5 than the surface slopes. This property makes the ASIS an excellent platform for measuring vector fluxes, such as solar radiation. It is well known (Katsaros and DeVault 1986; McWhorter and Weller 1991) that a tilting solarimeter yields a biased estimate of the mean flux. In addition to slope induced rms tilts, buoys are subject to mean tilts caused by windage, currents, etc. The ASIS mean tilts were found to be roughly double the rms tilts and highly correlated to the wind forcing (wind speed squared; see Fig. 10b). As the mean tilt is recorded, measurements subject to mean tilt-induced errors can be readily corrected. Finally, we note that the mean tilt of the buoy could reduce the range of the wave wire measurements. The expected mean tilt
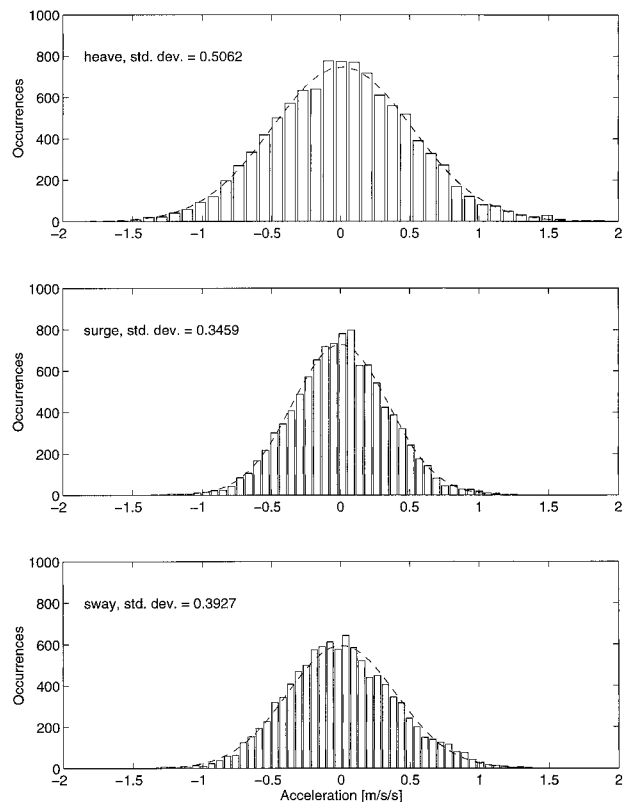


FIG. 9. Histograms of acceleration for the three orthogonal axes. Top panel: heave; middle panel: surge; bottom panel: sway. In each case the dashed curve is the Gaussian distribution with the same mean and standard deviation.
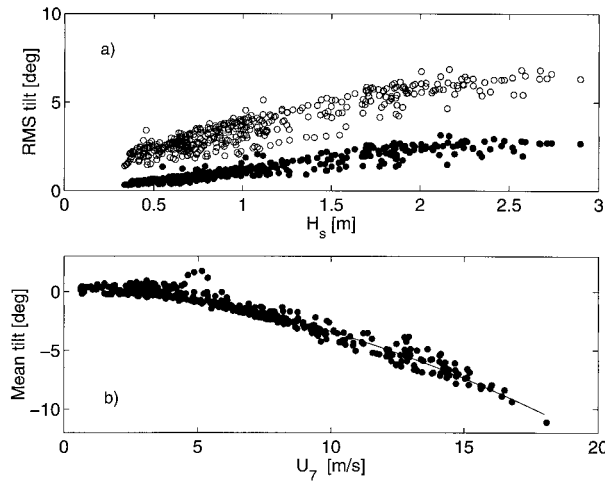
Fig. 10. (a) Surface (open circles) and ASIS (closed circles) rms tilts vs significant wave height. (b) Mean tilt of ASIS vs wind speed.

will be roughly 12° at wind speeds of 20 m s⁻¹, and the effective wave staff length is reduced by only 2%. In addition, at these tilt angles the mean water level at the outer wave staffs will shift by about 20 cm. Hence the mean tilt will not degrade wave measurements until considerably higher winds.

## 5. Measurements

### a. ASIS wave and wind measurements

The measurement period used here for illustration is the period near the peak of the frontal system of 23 April 1997 when the largest significant heights ($H_s$ = 2.92 m) were recorded and the wind speed at 5-m height was 12.7 m s⁻¹.

Figure 11a shows the measured wave spectrum and a line illustrating compliance with the well-established $f^{-4}$ power law from the peak at about 0.12 to 3.25 Hz. The spectra of wind components, as measured by the sonic anemometer and corrected for the buoy's motion (Anctil et al. 1994) are displayed Fig. 11b, displaced vertically by one decade for clarity. Note that the horizontal wind components have been rotated into the mean wind direction. All three components display well-defined −5/3 slopes at high frequencies, as expected in the inertial subrange. The cumulative cospectra of $-u'w'$ (downwind) and $-v'w'$ (crosswind) are graphed in Fig. 11c. In this case, the crosswind stress is near zero, so that the stress lies in the wind direction.

Figure 12 presents measured profiles of wind speed, obtained from the ASIS simultaneously with flux measurements of momentum. The four lower measurements are from 24-min averages of cup anemometer signals
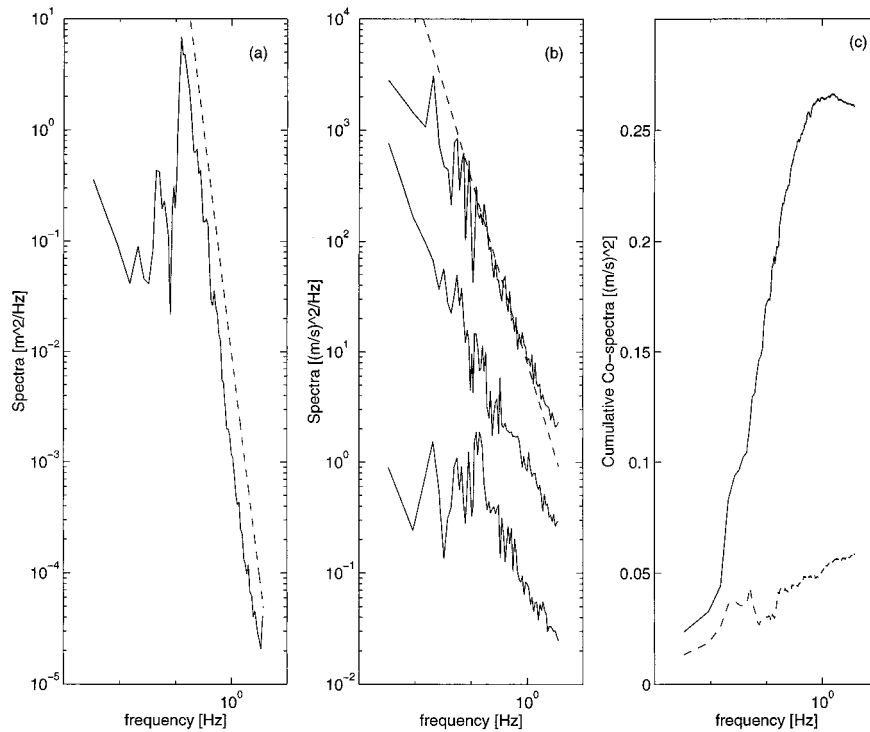


FIG. 11. (a) Surface displacement spectrum measured with ASIS buoy. The solid line is the wave energy spectrum and dashed line is proportional to $f^{-4}$. (b) Spectra of the three wind components ($100u$, $10v$, $w$) averaged over a 22.5-min record, the dashed line is proportional to $f^{-5/3}$; (c) Cumulative cospectra of the downwind (solid line) and crosswind (dashed line) components of the stress for a 22.5-min record. These three panels are derived from data in the height of the storm of 23 Apr 1997: $U_5$ = 12.7 m s⁻¹ and $H_s$ = 2.92 m.
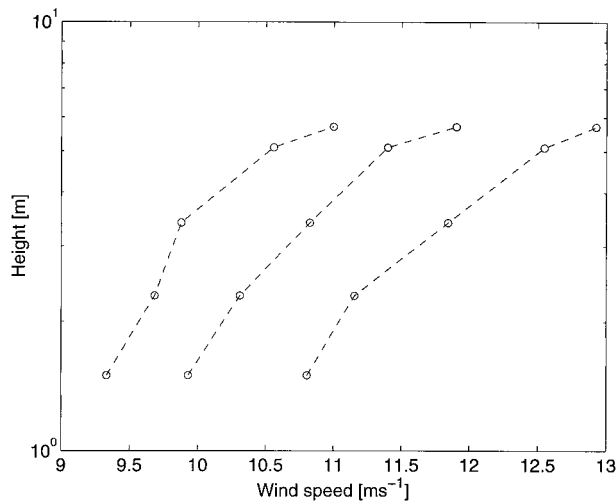
FIG. 12. Wind speed profiles (24 min) during the buildup of the storm of 23 Apr 1997 (0750, 0837, 0925 UTC). The sonic anemometer provided the top speed estimate; the other four levels are cup anemometers.



FIG. 13. Comparison of meteorological and wave parameters as measured by the ASIS buoy and the nearby NDBC 3-m discus (○): (a) atmospheric pressure; (b) wind speed via cup at 5.1 m (solid), 5.7 m sonic (dashed), and 4 m NDBC propeller; (c) wind direction at 4 m; (d) solar radiation; (e) air temperature; (f) sea surface temperature; and (g) significant wave height.

measured at 1 Hz. No corrections are made for the effects of motion of the ASIS on the cup anemometers. The top level is the 22.5-min average horizontal speed from the acoustic anemometer sampled at 15 Hz and with all motion corrections.

### b. Comparison with NDBC 3-m discus

Figure 13 illustrates a comparison of the ASIS measurements with those of the nearby NDBC 3-m discus (station 42036) for the 4-day period of 21–25 April 1997. The ASIS atmospheric pressure measurements were corrected for an offset of 4.7 mb due to an unresolved calibration issue. The very close agreement between the ASIS and NDBC pressure observations are shown in Fig. 13a. Figure 13b shows excellent agreement between the ASIS cup wind speed at 5.1-m height and the NDBC buoy's anemometer at 4 m. The ASIS cup measurements are 3-min averages of 1-Hz data, and the NDBC measurements are 10-min averages obtained once per hour. The NDBC data (open circles) fall within the scatter of the 3-min averages in almost all cases. Although not evident on the figure, the sonic anemometer speeds (dashed line) at 5.7 m, are higher than the 4-m NDBC speeds. A regression for wind speeds greater than 3 m s$^{-1}$, and excluding the peak of the 23 April storm yields $U_4^{\text{NDBC}} = 0.95U_{5.7}^{\text{ASIS}} + 0.08$ (correlation coefficient 0.977; 225 points). This difference is expected due to the height differential of the sensors in a logarithmic boundary layer.

Figure 13c shows excellent agreement between the ASIS wind direction and the NDBC buoys. The latter is a 10-min average obtained once per hour, while the former is a 22.5-min average. In the NDBC buoy the relative wind direction from a vane is added to the com-
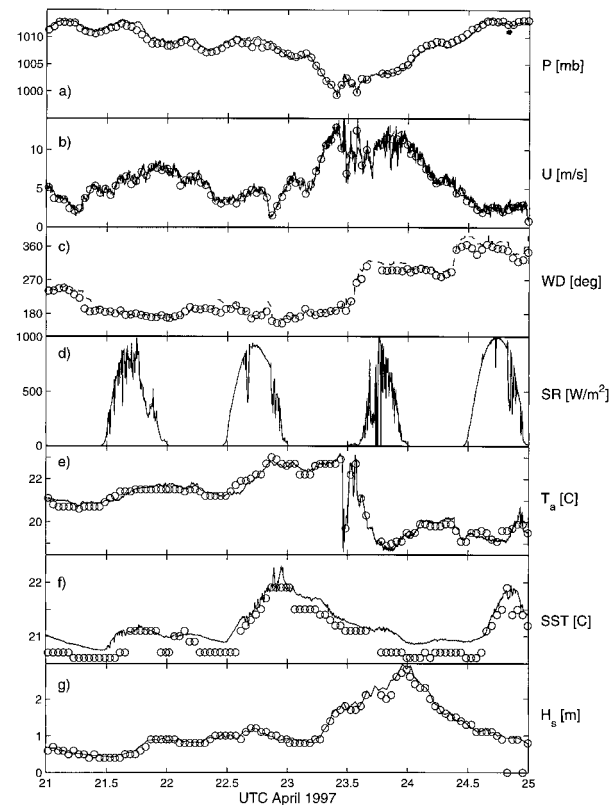
pass heading of the buoy, while the ASIS combines buoy heading with the relative direction obtained from the sonic anemometer.

The comparison of the two measurements of sea surface temperature (Fig. 13f) is good considering that the entire range of variation over this period is less than 2°C and the resolution of the NDBC system is only 0.1°C. Mesoscale variability in sea surface temperature would further confound this comparison. The effect of solar radiation (Fig. 13d) on the diurnal increases in SST is apparent as is the suppression of the radiative warming caused by wind mixing.

Atmospheric pressure and air temperature (Figs. 13a,e) show good agreement between the two buoys. Just before 1200 UTC on 23 April, the 4°C drop in air temperature and rapid return in about 2 h was caused by the passage of an extremely brief and intense wind event—perhaps a squall line—seen by the ASIS profile system as a rise of the 3-min average wind from 10 to almost 19 m s$^{-1}$ and sustained for only a few minutes. At the same time the solar radiation (Fig. 13d) was almost completely obscured.
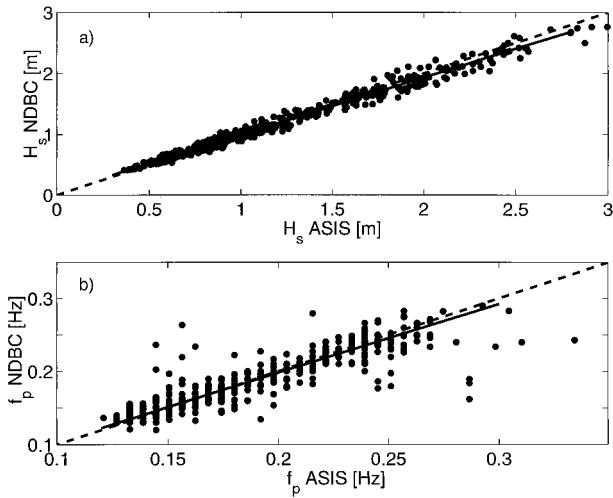
The correspondence between significant height mea-

FIG. 14. Scatterplot comparing (a) significant wave height and (b) peak frequency measured by ASIS buoy and NDBC 3-m discus. The dashed line corresponds to the 1-to-1 slope and the solid line is a linear regression.

surements from the two systems (Fig. 13g) is close. Over the full 19-day period depicted in Fig. 3, the two measurements were well correlated (correlation coefficient, 0.992; 507 points), with a regression between the two yielding $H_s^{\mathrm{NDBC}} = 0.94 H_s^{\mathrm{ASIS}} + 0.05$ (Fig. 14a). Here we have low-passed the ASIS data at 0.4 Hz for equivalency with the NDBC data. Similarly the mean periods (not shown) also track well, although there is a tendency of the NDBC buoy to overestimate the mean periods (i.e., underestimate the mean frequencies) of high-frequency waves. This is due to estimating the mean period as the ratio of the zeroth and first spectral moments, and the fact that the latter is underestimated through the high wavenumber (and hence frequency) cutoff imposed by the $O(3$ m) size of the NDBC discus. This underestimate obviously worsens as the mean period approaches the cutoff. Figure 14b shows the comparison of the peak frequency determined from the two buoys over the period 7–25 April. For comparison, the ASIS data have been binned in frequency, and the NDBC data inter-

polated onto the ASIS sample times. Much of the scatter occurs during situations with bimodal seas, where more than one spectral peak exists. The correlation coefficient (0.958) and regression line ($f_p^{\mathrm{NDBC}} = 0.94 f_p^{\mathrm{ASIS}} + 0.01$; 476 points) were calculated after removing these cases.

In Table 2 we summarize the comparison of the ASIS measurements with those from the nearby NDBC buoy recorded from 3 April to 6 May 1997. To minimize differences due to timing and sampling schedules, we computed averages from the higher resolution ASIS data to be equivalent with NDBC's sampling intervals and times. Table 2 reveals several noteworthy facts. 1) The correlation coefficients generally exceed 0.95, 2) the sign change of the mean error between cups 3 and 4 is consistent with the altitude of the NDBC wind sensor and boundary layer theory, 3) the rms error for wind speed is well below 1 m s$^{-1}$, and 4) the rms error for temperature is only about 0.25°C.

Finally (in Fig. 15) we compare directional wave spectra from the two buoys around 1430 UTC 8 April 1997. All spectra have been calculated using the maximum likelihood method. The top panels show the energy around the spectral peak. The bottom panels show the higher-frequency behavior, where the spectra have been multiplied by $f^5$ to show the equilibrium range. Again the comparison is good through the high frequency cutoff of the NDBC 3-m buoy (approximately 0.35 Hz). A more detailed comparison of directional wave spectra from ASIS and conventional buoys will be presented elsewhere.

## 6. Summary

We have constructed a new general-purpose buoy platform, specifically designed for air–sea interaction studies. The design was driven by the need for both high-resolution directional wave measurements over a wide range of wavelengths, and for accurate measurements of air–sea fluxes coincident with wave observations and other relevant parameters in the upper ocean layer. These considerations require a stable platform and led to a choice of a sparlike buoy. The dynamic range

TABLE 2. Comparison between ASIS and NDBC buoy measurements from 3 Apr to 6 May 1997. Note the large bias in the barometric pressure is due to an unresolved calibration issue with the ASIS sensor. All the air temperature sensors had very similar characteristics and here we show only results of the top sensor.

| Parameter | Mean error | rms error | Correlation coefficient | Number of points |
|---|---|---|---|---|
| Wind speed 1: $U_{1.5}$ [m s$^{-1}$] | −0.76 | 1.16 | 0.947 | 509 |
| Wind speed 2: $U_{2.3}$ [m s$^{-1}$] | −0.43 | 0.95 | 0.952 | 509 |
| Wind speed 3: $U_{3.4}$ [m s$^{-1}$] | −0.20 | 0.83 | 0.957 | 509 |
| Wind speed 4: $U_{5.1}$ [m s$^{-1}$] | 0.09 | 0.87 | 0.953 | 509 |
| Sonic speed: $U_{5.7}$ [m s$^{-1}$] | 0.15 | 0.63 | 0.975 | 160 |
| Sonic direction: $\theta$ [°] | 10.3 | 12.9 | 0.983 | 160 |
| Air temperature 4: $Ta_{4.9}$ [°C] | 0.05 | 0.26 | 0.989 | 507 |
| Water temperature: $Tw_{-0.8}$ [°C] | 0.21 | 0.25 | 0.985 | 502 |
| Barometric pressure: $P_{\mathrm{atm}}$ [mb] | 4.70 | 0.61 | 0.991 | 509 |
| Significant wave height: $H_s$ [m] | 0.02 | 0.09 | 0.989 | 508 |
| Peak frequency: $f_p$ [Hz] | 0.00 | 0.01 | 0.959 | 467 |
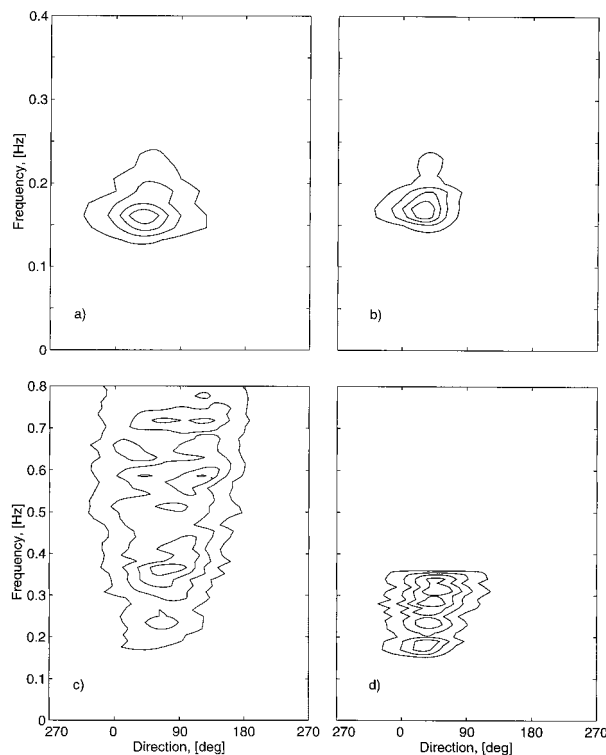
FIG. 15. Directional wave spectra as measured by (a), (c) the ASIS buoy and nearby (b), (d) NDBC 3-m discus buoy around 1430 UTC 8 Apr 1997. Calculations use the maximum likelihood method: (c), (d) show the spectra multiplied by $f^5$ to emphasize the equilibrium range.

of interfacial sensors further dictated that the buoy follow the large amplitude, low-frequency heaving motion of the surface. This, combined with the desire to minimize the buoy's disturbance to the air- and water-side boundary layers, led to a design consisting of several spar members along the perimeter of an open cage. This multicolumn arrangement provides not only the desired stability characteristics, but also a relatively open and unobtrusive structure. The buoy construction is modular, and when disassembled fits inside a standard 20-ft shipping container. Finally, it can be used in both a drifting or tethered mode. When tethered, it is attached to a conventionally moored tether buoy that itself can be used to deploy sensors over the full water column and to provide additional power and data storage capacity.

The tethered buoy system was field tested in the Gulf of Mexico, west of Tampa Bay, Florida, and in the western Mediterranean Sea. This sea trial demonstrated the seaworthiness of the moored buoy system in winds over 18 m s$^{-1}$, and seas in excess of 3-m significant heights. Measured response functions indicate that the buoy will follow waves longer than 7 s with good vertical stability, and thus the buoy should be capable of providing accurate measurements in much more severe sea states than those tested so far. The momentum fluxes, wind profiles, and wave directions derived from the buoy measurements are of high quality, and demonstrate the capability of the spar in open ocean conditions.

REFERENCES

Anctil, F., M. A. Donelan, W. M. Drennan, and H. C. Graber, 1994: Eddy correlation measurements of air–sea fluxes from a discus buoy. *J. Atmos. Oceanic Technol.,* **11,** 1144–1150.

Barstow, S. F., G. Ueland, H. E. Krogstad, and B. A. Fossum, 1991: The Wavescan second generation directional wave buoy. *IEEE J. Oceanic Eng.,* **16,** 254–266.

Bax, J. D., and K. J. C. de Werk, 1974: A floating storage unit designed specifically for the severest environmental conditions. SPE Paper 4853, 10 pp. [Available from Society of Petroleum Engineers of AIME, 6200 North Central Expressway, Dallas, TX 75206.]

Brown, R. G., and P. Y. C. Hwang, 1997: *Introduction to Random Signals and Applied Kalman Filtering.* 3d ed. John Wiley and Sons, 483 pp.

Businger, J. A., J. C. Wyngaard, Y. K. Izumi, and E. F. Bradley, 1971: Flux–profile relationships in the atmosphere surface layer. *J. Atmos. Sci.,* **28,** 181–189.

Capon, J., 1969: High-resolution frequency–wavenumber spectrum analysis. *Proc. IEEE,* **57,** 1408–1418.

Cavaleri, L., and E. Mollo-Christensen, 1981: Wave response of a

spar buoy with and without a damping plate. *Oceanic Eng.,* **8,** 17–24.

Donelan, M. A., J. Hamilton, and W. H. Hui, 1985: Directional spectra of wind-generated waves. *Phil. Trans. Roy. Soc. London,* **315A,** 509–562.

Drennan, W. M., M. A. Donelan, N. Madsen, K. B. Katsaros, E. A. Terray, and C. N. Flagg, 1994: Directional wave spectra from a Swath ship at sea. *J. Atmos. Oceanic Technol.,* **11,** 1109–1116.

Fisher, F. H., and F. N. Spiess, 1963: FLIP Floating Instrument Platform. *J. Acoust. Soc. Amer.,* **35,** 1633–1644.

Graber, H. C., E. A. Terray, M. A. Donelan, J. C. Van Leer, and W. M. Drennan, 1995: A lightweight multi-spar buoy—Design and sea trials. University of Miami, Tech. Rep. RSMAS 95-009, 38 pp. [Available from Rosentiel School of Marine and Atmospheric Science, 4600 Rickenbacker Causeway, Miami, FL 33149.]

Halkyard, J., and E. H. Horton, 1996: Spar platforms for deep water oil and gas fields. *Mar. Technol. Soc. J.,* **30,** 3–12.

Katsaros, K. B., and J. E. DeVault, 1986: On irradiance measurement errors at sea due to tilt of pyranometers. *J. Atmos. Oceanic Technol.,* **3,** 740–745.

——, M. A. Donelan, and W. M. Drennan, 1993: Flux measurements from a Swath ship in SWADE. *J. Mar. Syst.,* **4,** 117–132.

McWhorter, M. A., and R. A. Weller, 1991: Error in measurements of incoming shortwave radiation made from ships and buoys. *J. Atmos. Oceanic Technol.,* **8,** 108–117.

Mollo-Christensen, E., and C. Dorman, 1971: A buoy system for air–sea interaction studies: Buoy design and operation. Massachusetts Institute of Technology Department of Meteorology Rep. MITSG72, 25 pp. [Available from MIT, 77 Massachusetts Ave., Cambridge, MA 02139.]

Monin, A. S., and A. M. Obukhov, 1954: Basic laws of turbulent mixing in the ground layer of the atmosphere. *Akad. Nauk SSSR Geofiz. Inst. Tr.,* **151,** 163–187.

Newman, J. N., 1963: The motions of a spar in regular waves. David Taylor Model Basin, Hydromechanics Lab. Rep. 1499, 30 pp. [Available from David Taylor Model Basin, Naval Surface Warfare Center, Carderock Division, 9500 MacArthur Blvd., West Bethesda, MD 20817.]

——, 1977: *Marine Hydrodynamics.* The MIT Press, 402 pp.

Steele, K. E., C.-C. Teng, and D. W. C. Wang, 1992: Wave direction measurements using pitch–roll buoys. *Ocean Eng.,* **19,** 349–375.

Tasai, F., K. Kawatate, M. Ohkusu, and W. Koterayama, 1980: A single point mooring spar buoy for measuring ocean waves. *Ocean Eng.,* **7,** 173–192.

Valenzuela, G. R., 1978: Theories for the interaction of electromagnetic and oceanic waves—A review. *Bound.-Layer Meteor.,* **13,** 61–85.